British Journal of Cancer

ARTICLE

Check for updates

Cellular and Molecular Biology

Neoadjuvant therapy alters the collagen architecture of pancreatic cancer tissue via Ephrin-A5

Kosei Nakajima[1,2], Yoshinori Ino[1,2], Chie Naito[1,2], Satoshi Nara[3], Mari Shimasaki[1,2], Utako Ishimoto[1,2], Toshimitsu Iwasaki[1,2,3], Noriteru Doi[1,2], Minoru Esaki[3], Yoji Kishi[3], Kazuaki Shimada[3] and Nobuyoshi Hiraoka[1,2]✉

BACKGROUND: The treatment of pancreatic cancer (PDAC) remains clinically challenging, and neoadjuvant therapy (NAT) offers down staging and improved surgical resectability. Abundant fibrous stroma is involved in malignant characteristic of PDAC. We aimed to investigate tissue remodelling, particularly the alteration of the collagen architecture of the PDAC microenvironment by NAT.

METHODS: We analysed the alteration of collagen and gene expression profiles in PDAC tissues after NAT. Additionally, we examined the biological role of Ephrin-A5 using primary cultured cancer-associated fibroblasts (CAFs).

RESULTS: The expression of type I, III, IV, and V collagen was reduced in PDAC tissues after effective NAT. The bioinformatics approach provided comprehensive insights into NAT-induced matrix remodelling, which showed Ephrin-A signalling as a likely pathway and Ephrin-A5 (encoded by *EFNA5*) as a crucial ligand. Effective NAT reduced the number of Ephrin-A5$^+$ cells, which were mainly CAFs; this inversely correlated with the clinical tumour shrinkage rate. Experimental exposure to radiation and chemotherapeutic agents suppressed proliferation, *EFNA5* expression, and collagen synthesis in CAFs. Forced *EFNA5* expression altered CAF collagen gene profiles similar to those found in PDAC tissues after NAT.

CONCLUSION: These results suggest that effective NAT changes the extracellular matrix with collagen profiles through CAFs and their Ephrin-A5 expression.

British Journal of Cancer (2022) 126:628–639; https://doi.org/10.1038/s41416-021-01639-9

BACKGROUND

Pancreatic cancer (PDAC) has dire prognoses owing to potent distant metastasis and its highly invasive nature in surrounding tissues [1, 2]. Owing to its malignant nature, only 10–20% of pancreatic cancer patients are surgically treated, and recent guidelines suggest that surgery followed by adjuvant chemotherapy is the standard care for patients with relatively small resectable tumours [3, 4]. With regard to borderline resectable or locally advanced unresectable tumours, neoadjuvant therapy (NAT), i.e., pre-operative treatments such as S-1, gemcitabine, nab-paclitaxel, and the FOLFIRINOX regimen with/without radiation, is currently utilised and has been found to improve resectability [3, 5]. Meta-analyses show that, following NAT, approximately one-third of initially staged non-resectable tumours for surgical intervention were ultimately resectable [6, 7]. Furthermore, a recent multicenter phase III randomised control trial showed that neoadjuvant chemoradiotherapy prolonged patients' overall survival [8]. Thus, NAT is considered advantageous for the shrinkage of tumour volume and increases the possibility of surgical resection, thereby contributing to a better prognosis.

In PDAC tissue exposed to NAT, this treatment has been found to modulate the tumour immune microenvironment, which may induce antitumor immunity [9–13]. Furthermore, previous studies have shown that neoadjuvant chemotherapy was reported to reduce the number of cancer-associated fibroblasts (CAFs) [14]. CAFs contribute to providing a tumour-supporting microenvironment [15] and change their phenotype in association with the characteristics of the microenvironment [16]. CAFs produce a variety of components of the extracellular matrix in the tumour microenvironment such as fibronectin, hyaluronan, laminin, and collagens, whereby type I, IV, or V collagen promote the malignant phenotype of PDAC [17–21]. The production of collagen may be regulated by upstream gene, Ephrin-A5, which have been implicated in an in vitro experiment with cultured murine fibroblast cells [22]. Thus, the tissue content of several collagens contributes to PDAC progression. Nevertheless, collagen matrix alteration after NAT is yet to be investigated, and it was hypothesised that dynamic remodelling may occur in response to chemotherapy and radiation.

In this study, we provide evidence that NAT reduced the production of collagen fibres in CAFs, which were involved in the signal pathway via Ephrin-5. The remodelling of collagen in the microenvironment may allow the surgical removal of PDAC.

[1]Division of Molecular Pathology, National Cancer Center Research Institute, Tokyo, Japan. [2]Department of Analytical Pathology, National Cancer Center Research Institute, Tokyo, Japan. [3]Hepato-Biliary and Pancreatic Surgery Division, National Cancer Center Hospital, Tokyo, Japan. ✉email: nhiraoka@ncc.go.jp

Received: 28 September 2020 Revised: 26 October 2021 Accepted: 10 November 2021
Published online: 25 November 2021

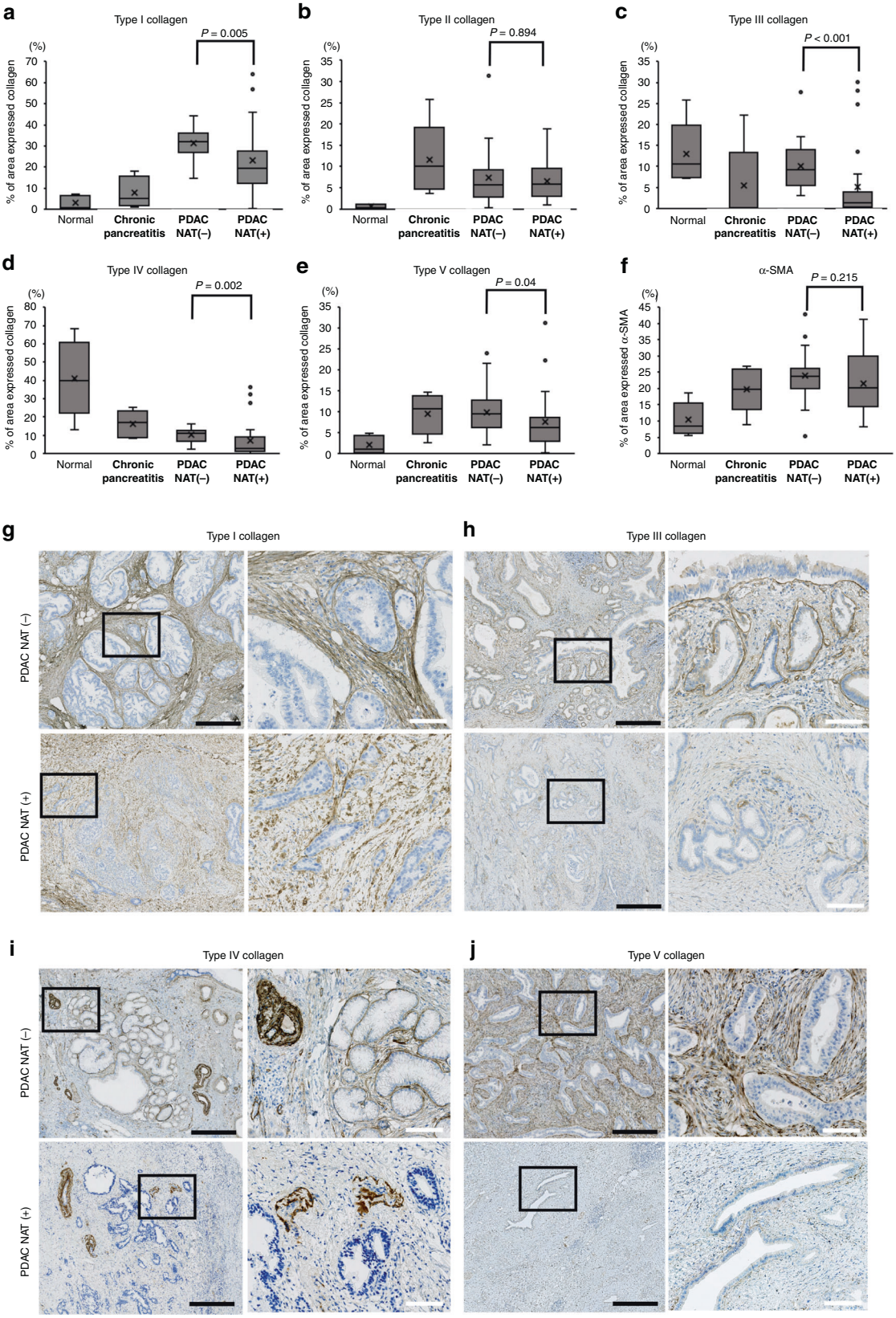

METHODS

Patients and samples

Clinical and pathological data were obtained through a detailed retrospective review of the medical records of 25 patients with PDAC who had undergone NAT followed by surgical resection between 2009 and 2017 at the National Cancer Center Hospital. We obtained fresh frozen tissues from resected surgical specimens, which were cut into 1.0-cm^3 sections, immediately frozen in Tissue-Tek OCT compound (Sakura Fineteck Japan,

Fig. 1 Comparison of the collagen-expressed area in the four pancreatic conditions. a–f The area occupied by the collagens and alpha-smooth muscle actin (α-SMA) was quantified using an automatic image analyzer after immunohistochemistry. Four pancreatic conditions were compared; normal pancreas ($n = 5$), chronic pancreatitis ($n = 5$), pancreatic cancer (PDAC) without neoadjuvant therapy (NAT) ($n = 20$), and PDAC with effective NAT ($n = 25$). Mann–Whitney *U* test was used for statistical analysis. **g–j** Immunohistochemical findings of collagens in PDAC tissues with or without NAT. For comparison, a pair of PDAC cases with effective NAT or without NAT is displayed. The left picture shows the low-power view, and the right picture shows the high-power view corresponding to the field of black square in the left picture. Black bars = 500 μm. White bars = 100 μm.

Tokyo, Japan), and stored at −80 °C until use. Clinical information, including treatments administered and their effects, of the patients are summarised in Supplementary Table S1. The median period after the initiation of NAT to surgery was 8.0 months (3.0–35.2 months), and the median response rate was 33.3%. Of the 25 patients, 64% showed a partial response (PR) ($n = 16$), and 36% showed stable disease (SD) ($n = 9$) based on the RECIST criteria [23]. The control comprised samples from 20 patients with PDAC who had undergone surgical resection between 2009 and 2017 at the National Cancer Center Hospital. Additionally, we used normal pancreatic tissue and chronic pancreatitis tissue (obstructive pancreatitis) that was histopathologically confirmed and was obtained from over 2 cm away from the cancer cells in the surgically resected pancreas. For validation, we used fresh frozen PDAC tissues from 39 patients with PDAC who had undergone NAT followed by surgical resection between 2019 and 2021, and from 39 patients (control) with PDAC without NAT followed by surgery. The demography of these patients is shown in Supplementary Table S2. The median period after initiation of NAT to surgery was 2.3 months (1.1–8.0 months), and the median response rate was 15.6%. Of the 39 patients with PDAC who had undergone NAT, 21% showed a partial response (PR) ($n = 8$), and 79% showed SD ($n = 31$).

Pathological examination

All carcinomas were examined pathologically and classified according to the World Health Organization classification [2], the Union for International Cancer Control TNM classification [24], and the Classification of Pancreatic Carcinoma of the Japan Pancreas Society [25]. The treatment effect was evaluated according to the examination protocol of the College of American Pathologists (https://documents.cap.org/protocols/cp-pancreas-exocrine-2016-v3301.pdf). Surgically resected specimens were fixed in 10% formalin and cut into serial slices (5-mm thick) horizontally in the pancreas head and sagittally in the pancreas body and tail. All sections were subjected to pathologic examination after staining with hematoxylin and eosin.

Immunohistochemistry

Immunohistochemistry was performed on formalin-fixed, paraffin-embedded tissue sections using the avidin-biotin complex method as described previously [26]. The antibodies used in this study are summarised in Supplementary Table S3. For quantitative assessments of the immunohistochemical results, the slide images were scanned with NanoZoomer 2.0-HT (Hamamatsu photonics, Hamamatsu, Japan); then, the stained area and numbers of positive cells or extracellular matrix were analysed using Tissue Studio (Definiens, Munich, Germany) to minimise interobserver variance [27]. DAB (3,3′-diaminobenzidine) and HistoGreen (Linaris Biologische Produkt, Dossenheim, Germany) were used as chromogens for double immunohistochemistry.

Immunofluorescence

Immunofluorescence was performed using formalin-fixed paraffin-embedded tissue sections and CAFs cultured on chamber slides, as described later. TrueView™ (Vector, Burlingame, CA) was used to quench the autofluorescence. AlexaFluor 488- and 594-conjugated antibodies were used as secondary antibodies. The immunofluorescence images were obtained using a BZ-X710 all-in-one fluorescence microscope (Keyence, Osaka, Japan).

Microarray analysis

Fresh frozen tumour tissue sections were sliced using cryostat, and total RNA was extracted from them using RNeasy Mini kits (Qiagen, Hilden, Germany). Thereafter, the RNA integrity number (RIN) was evaluated using a 2100 Bioanalyzer (Agilent, Santa Clara, CA), and the values were confirmed as >8.0. Microarray analysis was performed at the Chemical Evaluation Research Institute (CERI, Tokyo, Japan). Briefly, following Agilent's One-Color Microarray-Based Gene Expression Analysis Low Input Quick Amp Labeling ver. 6.9 protocol, an input of 100 ng of total RNA was used to generate Cy3-labelled cRNA. Subsequently, the samples were hybridised on SurePrint_G3_Human_GE_8x60K_Microarray ver.3.0 (Agilent). The arrays were scanned using the DNA Microarray Scanner (Agilent), and the acquired images were then quantified by Feature Extraction ver.10.7.1.1 (Agilent). The signals were normalised using Gene Spring GX14.5 (Agilent). To compare two groups of samples, i.e., PDAC tissue with/without NAT, Welch's *t*-test was used to determine statistical significance. The statistically significant genes were classified into the upregulated gene or downregulated gene groups. The data were separately imported into Ingenuity Pathway Analysis (IPA) ver. 43605602 (Qiagen), and canonical pathway analysis was performed using the Core Analysis program. Hierarchical clustering of the gene expression data was performed by a list on Gene Ontology. Regarding extracellular matrix-associated molecules, the gene list was made based on GO:0031012 (GO term: extracellular matrix). With regard to fibroblast-associated molecules, the gene list was combined with GO:0010761 (GO term: fibroblast migration), GO:0048144 (GO term: fibroblast proliferation), GO:0072537 (GO term: fibroblast activation), and GO:0044346 (GO term: fibroblast apoptotic process).

Tumour microenvironment analysis software

An online open-source software was used to visualise novel cell-to-cell interaction networks using the Cap Analysis of Gene Expression (CAGE) database, including 144 human primary non-cancerous cell types [28]. We extracted CAGE data (Dnaform, Kanagawa, Japan) from primary cultured cells, which were added to the software with more than 1500 CAGE data, including tumour cells in the FANTOM5 database. Subsequently, the database was enhanced to allow for the analysis of any tumour microenvironment with high scalability, enabling the inclusion of a further CAGE dataset of interest, termed 'Environmentome' (Amelieff, Tokyo, Japan). As this study focused on the pancreatic cancer microenvironment, we analysed the intercellular associations between PDAC cells and CAFs. For the expression data of PDAC and CAF, primary cultured patient-derived cells from surgical resection samples were used. The software has an integrated dataset program of ligand–receptor interactions pairs, obtained from the Database of Ligand−Receptor Partners (DLRP), International Union of Basic and Clinical Pharmacology (IUPHAR), Human Plasma Membrane Receptome (HPMR), Human Protein Reference Database (HPRD), Search Tool for the Retrieval of Interacting Genes/Proteins (STRING), and PubMed. In order to visualise the tumour microenvironment, among the numerous molecules, secretory proteins, plasma membrane proteins were included, whereas nuclear and cytoplasmic proteins were not selected based on the protein localization database (HGNC). In this analysis, we simultaneously examined all of the EFNA5 interacting molecules such as EPHA1, EPHA2, EPHA3, EPHA4, EPHA5, EPHA6, EPHA7, EPHA8, EPHB1, EPHB2, and EPHB6. To quantify the interaction strength of EFNA5 binding partners, we calculated the 'Expression Product,' which indicates (the expression level of ligand) × (the expression level of receptors) to represent the strength of the molecular association. The association was visualised by the software, leading to the identification of a significant relationship in the pancreatic cancer microenvironment.

Primary culture of CAFs

The procedure of the primary culture of CAFs has been previously described [16]. Briefly, fresh PDAC tissue was obtained during pancreatic surgery from PDAC patients without any pre-operative treatments. The tissue was cut into ~5–10 mm^3 pieces with scissors, and seeded in 6-cm^2 culture dishes with Dulbecco's modified Eagle's medium (DMEM) supplemented with 10% foetal calf serum. The pieces of tissue block were cultured at 37 °C in 5% CO_2 in a humidified atmosphere. The CAFs grew after 3–7 days in culture. After reaching confluence, the monolayers were trypsinized and passaged. The cultured CAFs between passages 2 and 4 were used for the subsequent experiments. To characterise the cultured cells and confirm them as CAFs, immunofluorescence and oil-red O staining were performed.

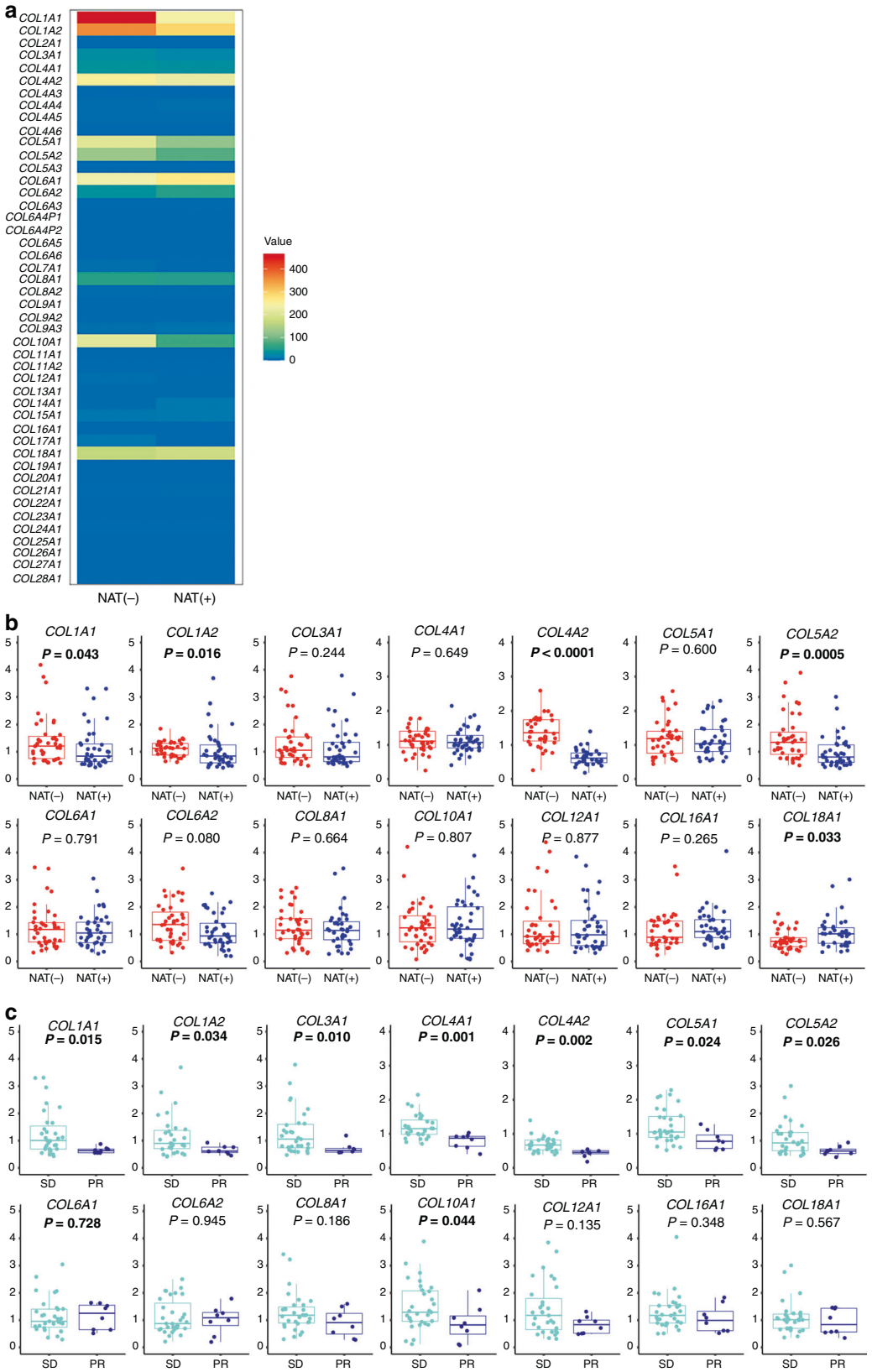

Cytotoxicity assay

The primary cultured CAFs were seeded into 96-well culture plates at a density of 1.5 or 3.0×10^4 cells per well, and incubated at 37 °C overnight. Thereafter, chemotherapeutic agents, oxaliplatin (Sigma), paclitaxel, 5-FU, gemcitabine, SN-38, an activate form of irinotecan (Selleck) were added in a dose-dependent manner (1 pM–100 μM), and incubated for 3 days. For radiation, the cells were exposed at 0 (control), 0.5, 1, 2, 4, 8, and 16 Gy of Co^{60}, and cultured for 1 week. At the end of each time period, the CCK-8

Fig. 2 Alteration of collagen gene expression following neoadjuvant therapy (NAT). a Transcriptional distribution of collagen gene profiles with effective NAT or without NAT. The heatmap shows the comparison of normalised/averaged values from *COL1A1* to *COL28A1* between four patients without NAT and four patients with NAT. **b**, **c** Collagen genes that are positively expressed in PDAC tissue (value of more than 50 in microarray data) or related to type I–V collagens are analysed using qRT-PCR analysis. The relative gene expression is compared between PDAC tissue with effective NAT ($n = 39$) and that without NAT ($n = 39$) (**b**), and between patients exhibiting SD after NAT ($n = 31$) and those exhibiting PR after NAT ($n = 8$) (**c**). Box plots and the scatter plots are combined. Whisker heights extend to 1.5 times the height of the box or, if no case/row has a value in that range, to the minimum and maximum values. The horizontal lines within the box indicate the median values. Differences were analysed by using Mann–Whitney *U* test. Bold letter indicates statistical significance.

reagent (Dojindo, Kumamoto, Japan) was added to cultured medium for 1 h, and the absorbance was measured at 450 nm using a microplate reader (Synergy H1, BioTek, Winooski, VT).

Quantitative RT-PCR (qRT-PCR)

Total RNA was extracted from CAFs cultured in 96-well culture plates using Cells-to-CT 1-step Taqman (Invitogen) or from CAFs cultured in 6-well culture plates using RNeasy Mini kits (Qiagen). qRT-PCR was performed on a Quantstudio 3 (Thermo Scientific, Foster city, CA, USA) system using a Taqman gene expression assay system (Thermo Scientific) or FastStart Universal Probe Master (ROX) with probes from the Universal Probe Library (Roche Diagnostics Corp., Indianapolis, IN, USA), as described previously [29]. The PCR primers and probes used are summarised in Supplementary Table S4. The CT values were normalised to that of GAPDH, and the ΔΔCT method was used to compare the expression levels of the genes.

Collagen genes expression after forced expression of EFNA5 in CAFs

To generate lenti-viral expression vectors, the total coding sequence of human *EFNA5* amplified by PCR with specific primers (5′-gAgTggCgCgTCggg-3′ and 5′-CTggTgTTCCAAgACCCTgA-3′) was sub-cloned into pCDH-CMV-MCS-IRES-Zeo-T2A-copGFP [30] to generate pCDH-CMV-MCS-IRES-Zeo-T2A-copGFP/huEFNA5. 293FT cells (Invitrogen) were co-transfected with psPAX2, pMD2.G, and pCDH-CMV-MCS-IRES-Zeo-T2A-copGFP/huEFNA5 or pCDH-CMV-MCS-IRES-Zeo-T2A-copGFP using Lipofectamine LTX with Plus reagent (Invitrogen) according to the manufacturer's instruction. Seventy-two hours after transfection, the culture supernatants were harvested and concentrated using Lenti-X Concentrator (Takara Bio, Kusatsu, Japan) as the virus solution. For viral infection and gene transduction, the primary cultured CAFs were seeded into 6-well culture plates at a density of 3.0×10^5 cells per well and cultured with the prepared viral solution (1:50) with polybrene (2–8 μg/mL) at 37 °C for 24 h. Viral-transduced cells were selected using Zeocin (Invitrogen) at 200 μg/mL for 10 days.

Collagen concentration

The collagen concentration of the culture supernatants was measured using a Quickzyme total collagen kit (Quickzyme Bioscience, Leiden, the Netherlands) according to the manufacturer's instructions.

Statistical analysis

For the quantification of immunohistochemistry data, a nonparametric analysis of variance test, the Mann–Whitney *U* test, was used to evaluate the statistical significance for the comparison of two categorical groups i.e., PDAC with/without NAT. With regard to the cellular experiments, significant differences were determined by two-sided *t*-tests. Differences at $P < 0.05$ were considered statistically significant. Statistical analyses were performed using IBM SPSS Statistics version 25.0 software (SPSS, Chicago, IL).

RESULTS

NAT reduced collagen volume in PDAC tissues

As collagens are the typical extracellular matrix components of PDAC and some are associated with malignant progression, [17–21, 31] we first immunohistochemically examined the manner in which the major collagen fibres, including type I–V collagens, change after effective NAT (determined as SD, PR, or complete response) [23]; the positively stained area was then quantified using an automatic image analyzer. To find out the possible clinical significance of the prevalent collagen fibre expression, we compared the percentage area to total tumour or pancreas area with four different pancreatic conditions: normal pancreas, chronic pancreatitis, PDAC without NAT, and PDAC after effective NAT (Fig. 1). Notably, there were significant differences in the ratio of collagen-expressed area between presence and absence of NAT. Overall, collagens noticeably tended to reduce the amount after NAT, particularly in type I ($P = 0.005$), type III ($P < 0.001$), type IV ($P = 0.002$), and type V collagen ($P = 0.040$), although not significantly in type II collagen ($P = 0.894$) and alpha-smooth muscle actin (SMA) ($P = 0.215$) (Fig. 1). Type I collagen fibres pathologically changed to crude fibres (Fig. 1g) and/or showed a hyaline degeneration-like appearance (Supplementary Fig. S1A) in the NAT-responded cases. Collagen type III intensely localised on the basement membrane surrounding PDAC cell nests in the native condition and partially disappeared in selected well-responded patients (Fig. 1h). Type IV collagen also composed the basement membrane surrounding cancer cell nests and vessel walls, which was reduced after NAT (Fig. 1i). Type V collagen was found in the cytoplasm of CAFs, and the expression was dramatically reduced in selected patients after NAT (Fig. 1j). These results suggested that NAT reduced major collagen volume.

We investigated the association between collagen reduction and tumour shrinkage after NAT and performed linear regression modelling to visualise this relationship. The nonparametric Spearman's rank correlation coefficient (ρ) was calculated to obtain a potential indication of the direction and strength of the linear association. There were no apparent correlations among collagen type I–IV, least of all for collagen type V; none of these were significantly different from zero, suggesting that type I–V collagens did not have strong associations with the tumour volume after NAT (Supplementary Fig. S2).

Ephrin-A signalling is a potential pathway for collagen alterations in PDAC tissues

The result of collagen reduction after effective NAT led us to comprehensively assess the changes in collagen. We performed a microarray analysis to analyse gene expression using total RNA extracted from the PDAC tissues of patients who underwent ($n = 4$) or who did not undergo NAT ($n = 4$). Genes coding for all types of collagen were included, i.e., COL1A1 to *COL28A1* (Fig. 2a). Genes encoding molecules that constitute types I, III, IV, and V collagens were less expressed in PDAC with NAT compared to PDAC without NAT. Among collagen genes, some (*COL6A1, COL6A2, COL16A1, COL18A1*) were more highly expressed and others (*COL8A1, COL10A1, COL12A1*) less so in PDAC with NAT compared to those in PDAC without NAT (Fig. 2a). To validate these findings, collagen gene expression was analysed in another cohort containing PDAC patients with effective NAT ($n = 39$) and no NAT ($n = 39$) (Supplementary Table S2) using qRT-PCR analysis (Fig. 2b). Among the collagen genes, *COL18A1* was more significantly highly expressed, and *COL1A1*, *COL1A2*, *COL4A2*, and *COL5A2* were comparatively significantly less expressed in PDAC with NAT compared to PDAC without NAT. Furthermore, among these patients with NAT, *COL1A1*, *COL1A2*, *COL3A1*, *COL4A1*, *COL4A2*, *COL5A1*, *COL5A2*, and *COL10A1* were significantly less expressed in patients exhibiting PR effect compared to those exhibiting SD

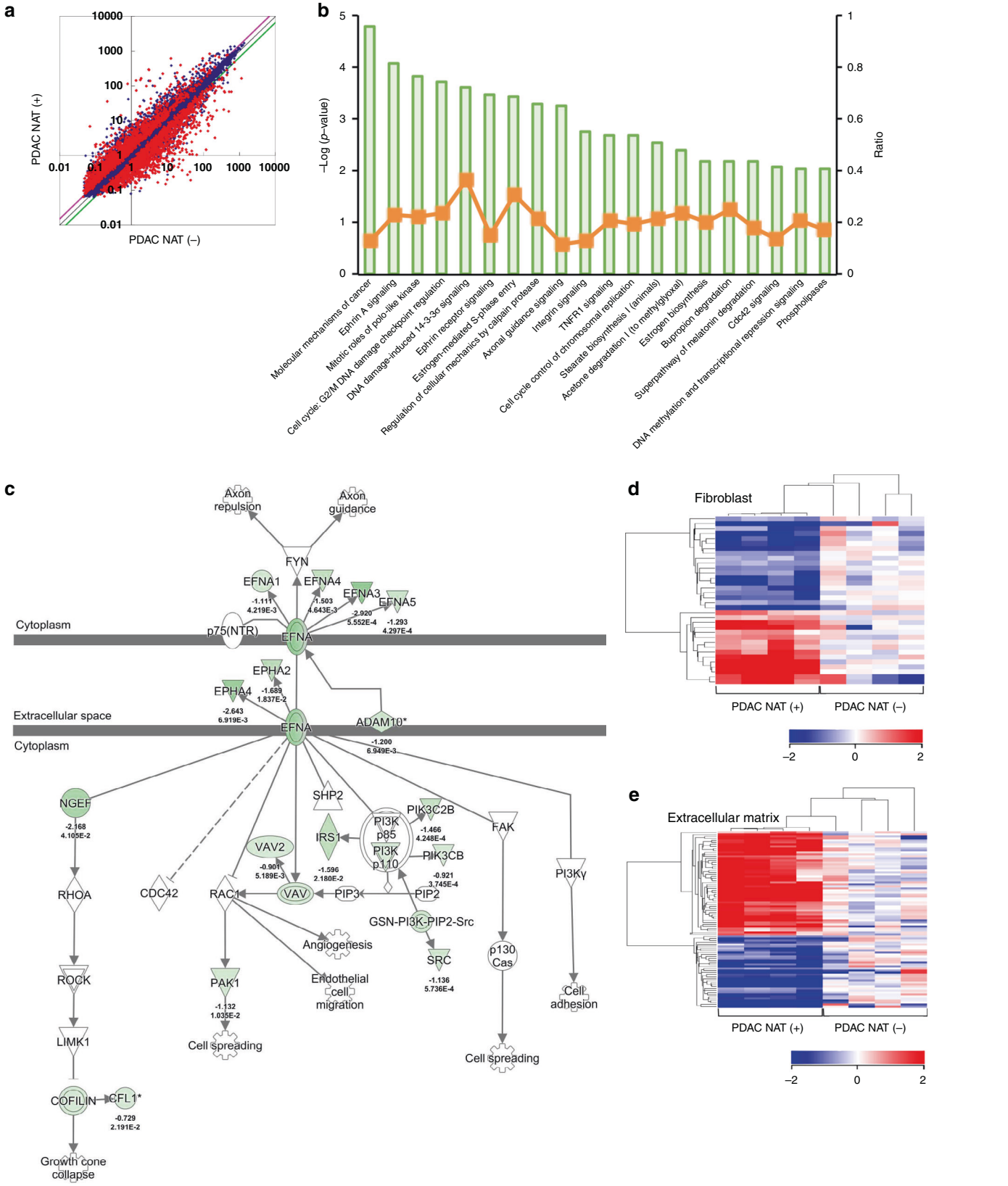

(Fig. 2c). These results indicated that the collagen constitution dynamically changed after effective NAT. They also suggested that the strength of the collagen alterations was associated with the effectiveness of the NAT.

The alteration of protein/transcript levels raised questions on the molecular mechanism(s) underlying such alterations of collagen profiles, which we examined by pathway analysis. First, scatter plot analysis showed that 1894 genes were significantly

Fig. 3 Visualisation of expressional profile and signalling after neoadjuvant therapy (NAT). a Scatter plot analysis of microarray datasets depict the altered expressional profiles of PDAC by effective NAT. *X* and *Y*-axis show averaged signal values. In total, 24,456 probes were examined. The red dots indicate expression of genes changed with statistical significance ($P < 0.05$) between the PDACs with effective NAT and PDACs without NAT, whereas the blue dots indicate genes whose expression altered without statistical difference. Purple and green lines indicate borders of 1.5- and 0.67-fold changes, respectively, in which 1894 genes were upregulated, and 1831 genes were downregulated by NAT. **b** Ingenuity pathway analysis revealed downregulated pathways by effective NAT. The pathways are ranked from the lowest *p* values (left) to higher (right). The green bars indicate –log (*p*-value) of each pathway, the strength of the statistical association is represented by the length of the bars. The orange lines indicate ratio value reflecting the proportion of gene elements in the differentially abundant gene list that corresponded to genes in each pathway. **c** Ingenuity pathway analysis depicted that the extracellular/intracellular signalling of Ephrin-A pathway. The result suggested that Ephrin-A1 (EFNA1), Ephrin-A3 (EFNA3), Ephrin-A4 (EFNA4), and Ephrin-A5 (EFNA5) were affected to EPHA2 and EPHA4 receptors, leading to cross-talking to PI3K, SRC, and others. **d**, **e** Heat map analyses delineate the dynamic alteration of the gene expression profile by NAT in fibroblast and extracellular matrix-associated genes.

upregulated, and 1831 genes were downregulated after effective NAT. This implies that NAT induced dramatic changes in PDAC cells and the microenvironment, including the collagens therein (Fig. 3a). Furthermore, to elucidate the changes in pathway/signalling after NAT, we employed bioinformatics software (IPA), to reconstruct the activated/suppressed pathways using selected statistically significant genes. The results showed that 106 pathways were upregulated, whereas 75 pathways were downregulated (Supplementary Table S5) ($P < 0.05$). Among these, Ephrin-A signalling and Ephrin receptor signalling were regarded as highly suppressed pathways and ranked 2nd and 6th, respectively (Fig. 3b); moreover, and Ephrin pathways have been implicated in matrix remodelling [32–34]. Ephrin-A signalling was delineated by the upstream ligands, i.e., the initiators of signalling, Ephrin-A1 (*EFNA1*), Ephrin-A3 (*EFNA3*), Ephrin-A4 (*EFNA4*), and Ephrin-A5 (*EFNA5*) (Fig. 3c). To visualise the overall change of the extracellular matrix and fibroblasts as a synthesiser of matrix components, we classified the statistically significant genes by gene ontology (GO). The expression of genes associated with fibroblasts and the extracellular matrix changed dynamically by effective NAT (Fig. 3d, e). Among these, consistent with the pathway analysis, the stratified bioinformatics approaches using heat map analysis nominated *EFNA5* as one of the relevant genes for extracellular matrix remodelling (Table 1). Since Ephrin-A5 has been implicated as an upstream regulator of collagen synthesis in murine fibroblasts [22], *EFNA5* downregulation by effective NAT may suppress collagen expression.

Table 1. Gene list of extracellular matrices downregulated after neoadjuvant therapy (NAT) in PDAC tissue.

Gene symbol	Gene name (Downregulated by NAT)	Fold Change
LGALS3BP	lectin, galactoside-binding, soluble, 3 binding protein	0.002
PCSK6	proprotein convertase subtilisin/kexin type 6	0.006
LAMB3	laminin, beta 3	0.007
ANXA2	annexin A2	0.011
LAMC2	laminin, gamma 2	0.012
EFNA5*	**ephrin-A5***	0.013
CASK	calcium/calmodulin-dependent serine protein kinase (MAGUK family)	0.013
ITGA6	integrin, alpha 6	0.021
MMP14	matrix metallopeptidase 14 (membrane-inserted)	0.021
CD151	CD151 molecule (Raph blood group)	0.025
LAMA3	laminin, alpha 3	0.025
PKM	pyruvate kinase, muscle	0.028
PLOD3	procollagen-lysine, 2-oxoglutarate 5-dioxygenase 3	0.031
SLPI	secretory leucocyte peptidase inhibitor	0.031
PLAT	plasminogen activator, tissue	0.032
LGALS3	lectin, galactoside-binding, soluble, 3	0.038
CST3	cystatin C	0.044
MMP28	matrix metallopeptidase 28	0.047
COL7A1	collagen, type VII, alpha 1	0.047
LOXL2	lysyl oxidase-like 2	0.048
MMP11	matrix metallopeptidase 11 (stromelysin 3)	0.051
IBSP	integrin-binding sialoprotein	0.053
ACHE	acetylcholinesterase (Yt blood group)	0.054
COL17A1	collagen, type XVII, alpha 1	0.064
NDNF	neuron-derived neurotrophic factor	0.070
DAG1	dystroglycan 1 (dystrophin-associated glycoprotein 1)	0.073
MMP12	matrix metallopeptidase 12 (macrophage elastase)	0.089
TINAG	tubulointerstitial nephritis antigen	0.093
BMP7	bone morphogenetic protein 7	0.099
AGRIN	agrin	0.102
MUC4	mucin 4, cell surface associated	0.175
DMBT1	deleted in malignant brain tumours 1	0.176

EFNA5 is nominated as a candidate (*).

Decrement of Ephrin-A5$^+$ cells was associated with tumour shrinkage by NAT

Strong Ephrin-A5 expression was found in the stromal cells in PDAC tissues by immunohistochemistry (Fig. 4a). There were few cells expressing Ephrin-A5 in normal pancreatic tissue and chronic pancreatitis tissue (Supplementary Fig. S1C–F). The abundance of Ephrin-A5$^+$ cells was notably reduced after NAT (Fig. 4b and Supplementary Figs. S1C–F). Ephrin-A5$^+$ cell density had an inversely and relatively strong association with tumour shrinkage in patients after NAT (Fig. 4c; $\rho = -0.466$; $P = 0.033$).

To determine the specific type of Ephrin-A5$^+$ cells, double immunostaining revealed that these cells expressed alpha-SMA and CD33, though no lymphoid lineage markers (CD4, CD8, CD19, CD20, CD138, FOXP3, TBX21), innate immune cell markers (CD56, EOMES, Bcl11b), neutrophil marker CD66b, macrophage markers (CD68, CD163, CD204), and CD14 (Supplementary Fig. S3). The majority of Ephrin-A5 was expressed in a part of the alpha-SMA$^+$ CAFs (Fig. 4d), and a minority of Ephrin-A5$^+$ cells was a part of the CD33$^+$ myeloid cells (Supplementary Fig. S4).

Interaction between Ephrin-A5 in CAFs and the Ephrin receptor (Eph) A2 in PDAC cells

We visualised the molecular interactions in the PDAC microenvironment using comprehensive transcript profiles from various components of the tumour microenvironment, and examined which molecules interacted with Ephrin-A5 bioinformatically using tumour microenvironment analysis software ('Methods'). The results suggested that Ephrin-A5 expressed in CAFs interacted with Ephrin receptor (Eph) A2 derived from PDAC cells (Fig. 4e). Additionally, the Ephrin-A5 in CAFs interacted with EphA2 and

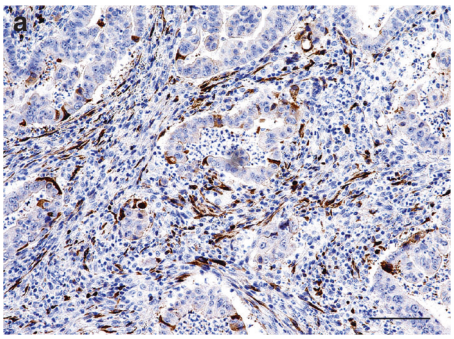

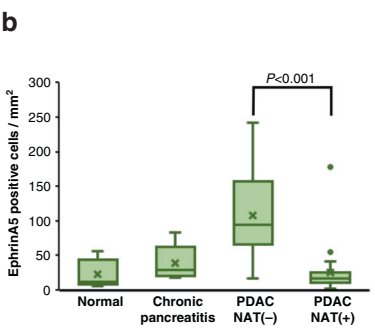

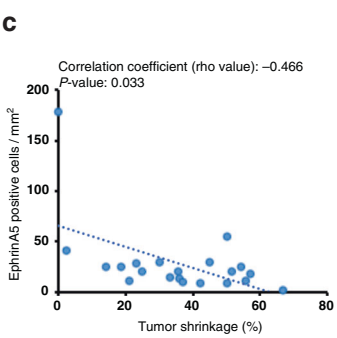

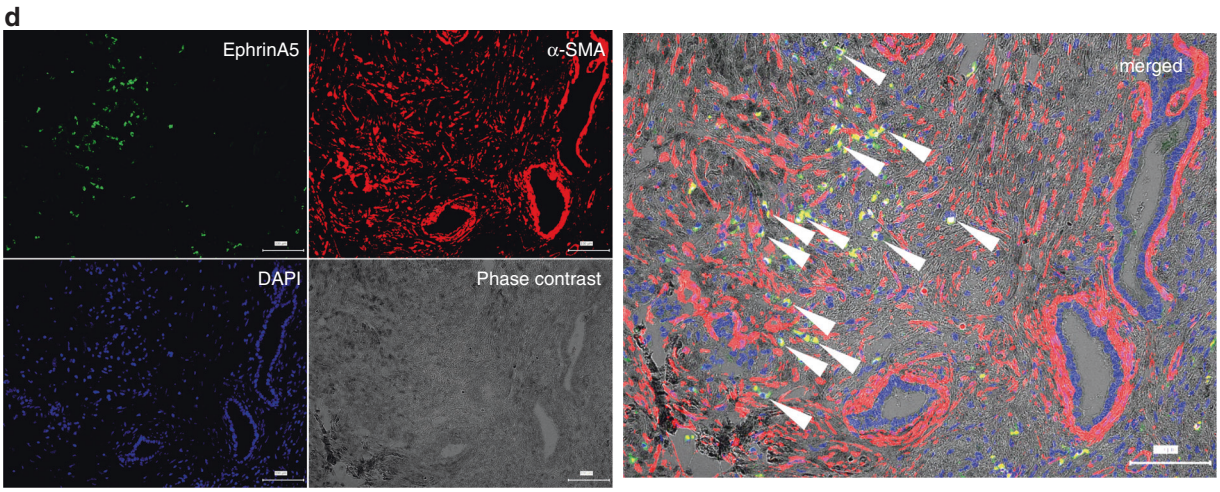

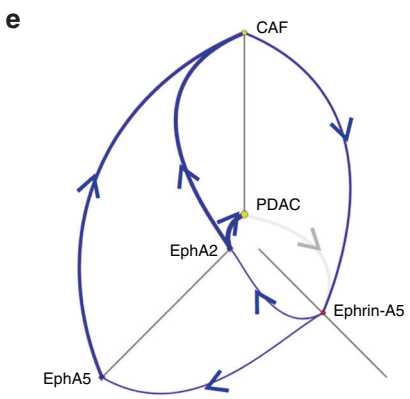

f

Intercellular/ligand–receptor association	Expression product (TPM)
CAFs →PDAC cells	
Ephrin-A5→EphA2	406.18*
CAFs → CAFs	
Ephrin-A5→EphA2	119.16
Ephrin-A5→EphA5	51.36

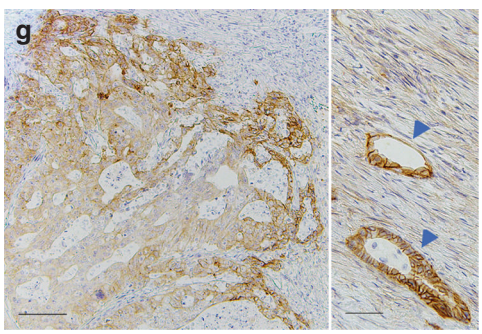

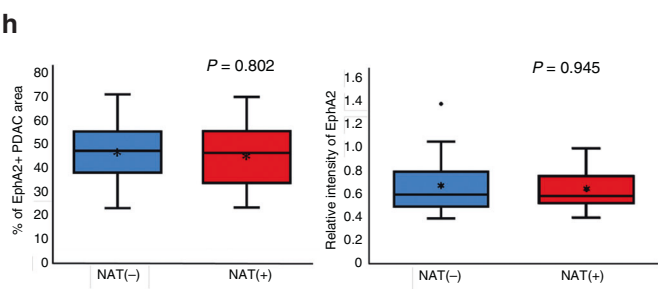

EphA5 of CAFs themselves. To quantify and highlight the significant molecular interactions, we calculated the value of the 'expression product,' which represented the strength of the molecular association. The association between Ephrin-A5 of CAFs and EphA2 of PDAC cells was the highest ranked value (Fig. 4f). It is suggested that the Ephrin-A5 pathway-related events are produced mainly by paracrine signals between CAFs and PDAC cells, and autocrine signals in CAFs.

Fig. 4 Neoadjuvant therapy (NAT) suppressed *EFNA5* positive cells in PDAC tissues. a Representative image of Ephrin-A5 immunohistochemistry in PDAC tissue. Ephrin-A5$^+$ cells were detected in the stroma in the PDAC tissue without NAT. Black bar = 100 μm. **b** Quantification of Ephrin-A5$^+$ cells based on immunohistochemistry results, Ephrin-A5$^+$ cell density was measured using an automatic image analyzer. Four pancreatic conditions were compared; normal pancreas ($n = 5$), chronic pancreatitis ($n = 5$), PDAC without NAT ($n = 20$), PDAC with effective NAT ($n = 25$). Mann–Whitney *U* test was used for statistical analysis. **c** Association between Ephrin-A5$^+$ cell density and tumour shrinkage. Linear regression modelling shows an inverse association between the two values (broken blue line). Spearman's rank correlation coefficient shows $\rho = -0.466$, which is statistically significant ($P = 0.033$). The blue dots indicate each patient value. **d** Immunofluorescence reveals that the majority of Ephrin-A5$^+$ cells express alpha-smooth muscle actin (α-SMA). White arrow indicates Ephrin-A5 and α-SMA double-positive cells in the tumour stroma in the merged image. **e** Visualising autocrine Ephrin-A5 signalling amplification in the PDAC microenvironment. Blue arrows indicate each expression and interaction, showing the feedback mechanism of Ephrin-A5 interaction. The strength of the association is represented by the thickness of blue arrows. **f** Relative strength of molecular association. The unit defines the counts per length of transcript kilobase per million (TPM) reads mapped. The values have been normalised in the cellular/molecular datasets of software, allowing the molecular expression levels to be compared. To quantify the association of ligand–receptor interactions of Ephrin-A5 (*EFNA5*), we calculated 'the value of ligand (TPM) × the value of receptor (TPM),' termed as 'expression product,' representing the strength of the ligand–receptor association. *Note that CAF highly interacted with PDAC cells via Ephrin-A5 (*EFNA5*)—Ephrin receptor A2 (EphA2, encoded by *EPHA2*). **g** Representative image of EphA2 immunohistochemistry of PDAC tissue. The EphA2 density in PDAC cells tends to be higher in the peripheral positions of the tumour nests (left column). EphA2 is sometimes expressed in CAFs (right column). Arrow heads indicate cancer cell nests. The black bars indicate 100 μm (left column) and 50 μm (right column). **h** Both of % of EphA2-positive PDAC cell area in PDAC tissue and mean relative intensity of EphA2 in PDAC tissues are not significantly changed between PDAC cases without NAT ($n = 20$) and with effective NAT ($n = 25$).

EphA2 expression in PDAC cells

EphA2 was immunohistochemically determined to be expressed almost all PDAC cases with various staining density. The EphA2 density in PDAC cells varied within the same case, although it tended to be higher in the PDAC cells at the invasive front, where PDAC cells often decreased their differentiation degree (Fig. 4g). EphA2 was also sometimes expressed in CAFs (Fig. 4g). EphA2 expression in PDAC cells was not significantly altered after effective NAT (Fig. 4h).

Ephrin-A5 contributes to collagen synthesis in CAFs

To ascertain the role of Ephrin-A5 in altering collagen synthesis in CAFs, we cultured CAFs derived from fresh PDAC tissue and analysed their expression of different types of collagen following a forced expression of *EFNA5* (Fig. 5a). Our primary cultured CAFs expressed vimentin and alpha-SMA, although no cells expressed cytokeratins and desmin (Supplementary Fig. S5). Oil-red O staining revealed no cells with oil droplets. The primary cultured CAFs, 20% of which expressed Ephrin-A5 weakly (Supplementary Fig. S6), were transduced with the *EFNA5* gene using a lentivirus vector. Upon the selection of the transduced cells (Supplementary Fig. S6), collagen genes that were positively expressed in PDAC tissue (value of more than 50 in microarray data) or related to type I–V collagens were analysed using qRT-PCR analysis. Increasing gene expression levels of *COL1A2, COL4A1, COL4A2*, and *COL8A1* and decreasing gene expression levels of *COL6A1, COL6A2, COL12A1, COL16A1*, and *COL18A1* were found. With the exception of *COL12A1*, these alterations were consistent with the expression after effective NAT in PDAC tissue (Fig. 2). These results suggested that some of the collagen chains are downstream effectors of the Ephrin-A5 signalling pathway.

Radiation and chemotherapeutic reagents reduced the number of CAFs and downregulated expression of *EFNA5* and collagen synthesis in CAFs

We examined the effects of NAT on the Ephrin-A5-collagen synthetic axis in CAFs. Primary cultured CAFs were treated with clinically available chemotherapeutic drugs or radiation. Radiation and chemotherapeutic drugs, paclitaxel, oxaliplatin, 5-FU, gemcitabine, and SN-38 (an active form of irinotecan) reduced the number of CAFs in a dose-dependent manner (Fig. 5b). Additionally, it is notable that non-cytotoxic low dose exposure of radiation and chemotherapy largely exerted reductions of the total collagen concentration in culture supernatants of CAFs (Fig. 5c). The low dose radiation and chemotherapeutic reagents also suppressed *EFNA5* expression in CAFs (Fig. 5d). These findings suggest that NAT reduces the number of CAFs in high dose exposure, and it is likely to downregulate *EFNA5* expression and total collagen synthesis in low dose exposure, which together may ultimately lead to tumour shrinkage as net results of NAT.

DISCUSSION

NAT has been reported to have certain therapeutic effects in reducing PDAC size; thus, it is considered a potential standard therapy [3, 5–8]. The tumour tissue matrix is involved in the formation of the clinicopathological and biological characteristics of cancer [17–21]. It is important to understand the effects of NAT on the tumour stroma of PDAC tissues, particularly for developing the next generation of combined therapy. In this study, we found that NAT induced remodelling of the tumour microenvironment of PDAC through the apparent reduction of some collagens that are involved in the malignant characteristics of this cancer [17–21]. We also demonstrated a possible mechanism for this remodelling, i.e., NAT reduces Ephrin-A5 expression in CAFs, resulting in a dramatic change in the collagen gene expression levels as an induction of a decrease in the collagen volumes in the PDAC microenvironment. Indeed, tumour shrinkage by NAT was significantly associated with the density of Ephrin-A5$^+$ cells in PDAC tissues. Furthermore, forced expression of *EFNA5* in CAFs altered collagen expression in a manner similar to that post NAT. It is suggested that NAT can remodel the tumour microenvironment through CAFs and the collagen-Ephrin-A5 signalling axis.

Ephrin receptors constitute the largest family of receptor tyrosine kinases, and some are expressed in PDAC. The ligands, *i.e.*, Ephrins, induce phosphorylation of the receptors, activating downstream signalling, which subsequently induces tumour growth, invasive potential, anoikis resistance, and metastasis of PDAC [35–37]. Ephrins have also been implicated in matrix remodelling [32–34]. Ephrin-A5 can bind to EphA2, A3, A4, A5, A6, A8, and B2 and activate the downstream signalling in physiological conditions [38, 39]. Bioinformatics analysis revealed that Ephrin-A5 in CAFs interacted to EphA2 and EphA5 of CAFs themselves and to EphA2 in PDAC cells, with the highest association of Ephrin-A5 in CAFs with EphA2 in PDAC cells. It is assumed that Ephrin-A5 signal in CAFs develops in a paracrine manner with PDAC cells, and possibly in autocrine manner with CAFs. In murine fibroblasts, Ephrin-A5 leads to the activation of Src family kinase Fyn, integrin-mediated adhesion, and Erk MAP kinase, thus enhancing fibroblast proliferation, migration, and collagen synthesis [22, 37]. In this study, we found that Ephrin-A5 did not induce all collagen genes altered by effective NAT in PDAC tissues, indicating that factors other than Ephrin-A5 are also involved in regulating collagen expression. EphA2 is a

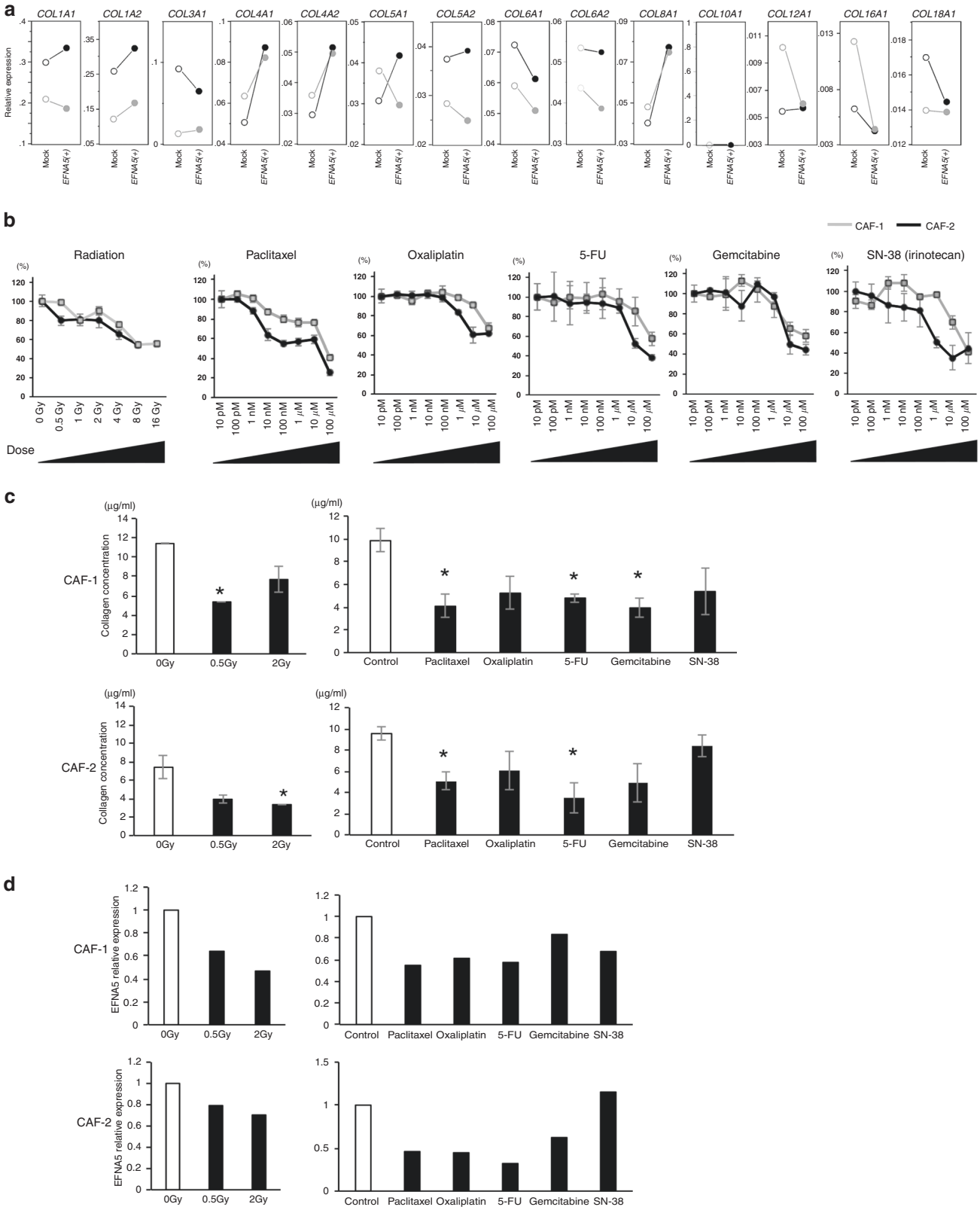

transmembrane tyrosine kinase that functions in the regulation of cell growth, survival, angiogenesis, and migration. Previous reports have shown that EphA2 is involved in the malignant characteristics of PDAC cells [40, 41] and functions as a tumour intrinsic driver to suppress host antitumor immunity [42]; however, to our knowledge, no report has shown that EphA2 relates to collagen formation through the interaction between PDAC cells and CAFs.

The synthesised collagens comprise the stromal matrix and basement membrane surrounding PDAC cell nests. Specifically, type I, III, IV, and V collagens were components of the basement

Fig. 5 Experimental exposure of cancer-associated fibroblasts (CAFs) to chemotherapeutic reagents or radiation. a Comparison of collagen gene expression between CAF forced expression of *EFNA5* and the control CAFs. CAFs were obtained from two PDAC cases (black and grey in graphs) each transduced with *EFNA5* or control vector (Mock). Gene expression was analysed by qRT-PCR, and the *Y*-axis indicates relative gene expression in the CAFs transduced with *EFNA5* gene or Mock. **b** Cytotoxicity testing of chemotherapeutic reagents or radiation to CAFs. CAFs originating from two different PDAC patients, CAF-1 (grey line) and CAF-2 (black line) were used in this study. Data represent the mean ± SD. **c** Collagen concentration after treatment of radiation and chemotherapy. Based on the results of cytotoxicity tests, the non-cytotoxic doses were determined: For radiation, 0.5 and 2 Gy were used. The following concentration of chemotherapeutic agents were used; 1 nM paclitaxel, 100 nM oxaliplatin, 1 nM 5-FU, 100 nM gemcitabine, and 20 nM SN-38 (an active form of irinotecan). Data represent the mean ± SD. White bars indicate non-treated CAFs (control), whereas black bars indicate collagen concentration after the treatments. Data represent the mean ± SD. $*P > 0.05$. **d** *EFNA5* expression after radiation and chemotherapy. White and black bars indicate the non-treated and treated CAFs, respectively.

membrane in this study, which is similar to that reported in a previous study [43]. Subsequently, the collagen fibres are recognised by PDAC cells expressing a wide variety of cell-surface molecules such as heterodimers of α- and β-integrins, specifically α2β1 integrin, resulting in cancer proliferation and migration [44, 45]. As such, collagen production by CAF and PDAC growth are chain reaction events in the context of the PDAC microenvironment [17–21, 31, 46]. Considering the linker role of collagens between cancer cells and CAFs, NAT may promise clinical benefits to insulate the malignant connection, halting PDAC progression. This study elucidated two advantages of NAT in extracellular matrix remodelling: 1) chemotherapeutic agents and radiation offer dose-dependent suppression of CAF, and 2) reduced collagen synthesis via Ephrin-A signalling may indirectly suppress PDAC progression.

The molecular mechanisms of chemotherapeutic reagents and radiation in reducing *EFNA5* expression in CAFs remain unknown. When these reagents inhibit cellular proliferation of both CAFs and cancer cells, signal pathways in cells, for example that of Ephrin-A, are modified. However, it is suggested that the presence of Ephrin-A5 expressed in CAFs might be a predictive marker for chemotherapy or radiotherapy including NAT, since it is a target for these treatments. Additionally, Ephrin-A5 in PDAC tissue may be applicable for monitoring effective chemotherapy or radiation.

There are some limitations to this study in that the data collection and analyses of our clinicopathological study were performed retrospectively using small cohorts. Although the NAT regimen has not been unified in the guidelines, the PDAC patients were enrolled without eligibility criteria and were not administered NAT uniformly. Hence, the variations in the NAT effects and host responses may be more diverse. Further studies are required to verify our findings in this regard.

In conclusion, NAT may be advantageous in suppressing collagen fibre remodelling in an attempt to halt the progression of incurable PDAC. The altered collagen components should be considered an integral part of NAT, whereby the findings may contribute to the advancement of surgical procedures.

DATA AVAILABILITY

The datasets used and analysed during the current study are available from the corresponding author upon reasonable request.

REFERENCES

1. Hidalgo M. Pancreatic cancer. N. Engl J Med. 2010;362:1605–17.
2. Hruban RH, Adsay NV, Esposito I, Fukushima N, Furukawa T, Kloeppel G, et al. Pancreatic ductal adenocarcinoma. In: Board WCoTE (ed.) World Health Organization Classification of Tumours. 5th Edition. Digestive System Tumours, 5th edn. IARCPress: Lyon, 2019, pp. 322–32.
3. Ducreux M, Cuhna AS, Caramella C, Hollebecque A, Burtin P, Goere D, et al. Cancer of the pancreas: ESMO Clinical Practice Guidelines for diagnosis, treatment and follow-up. Ann Oncol. 2015;26:v56–68.
4. Tempero MA. NCCN Guidelines updates: pancreatic cancer. J Natl Compr Canc Netw. 2019;17:603–5.
5. Tempero MA, Malafa MP, Al-Hawary M, Asbun H, Bain A, Behrman SW, et al. Pancreatic adenocarcinoma, Version 2.2017, NCCN clinical practice guidelines in oncology. J Natl Compr Canc Netw. 2017;15:1028–61.
6. Assifi MM, Lu X, Eibl G, Reber HA, Li G, Hines OJ. Neoadjuvant therapy in pancreatic adenocarcinoma: a meta-analysis of phase II trials. Surgery. 2011;150:466–73.
7. Gillen S, Schuster T, Meyer Zum Buschenfelde C, Friess H, Kleeff J. Preoperative/neoadjuvant therapy in pancreatic cancer: a systematic review and meta-analysis of response and resection percentages. PLoS Med. 2010;7:e1000267.
8. Tienhoven GV, Versteijne E, Suker M, Groothuis KBC, Busch OR, Bonsing BA, et al. Preoperative chemoradiotherapy versus immediate surgery for resectable and borderline resectable pancreatic cancer (PREOPANC-1): a randomized, controlled, multicenter phase III trial. J Clin Oncol. 2018;36:LBA4002.
9. Homma Y, Taniguchi K, Murakami T, Nakagawa K, Nakazawa M, Matsuyama R, et al. Immunological impact of neoadjuvant chemoradiotherapy in patients with borderline resectable pancreatic ductal adenocarcinoma. Ann Surg Oncol. 2014;21:670–6.
10. Murakami T, Homma Y, Matsuyama R, Mori R, Miyake K, Tanaka Y, et al. Neoadjuvant chemoradiotherapy of pancreatic cancer induces a favorable immunogenic tumor microenvironment associated with increased major histocompatibility complex class I-related chain A/B expression. J Surg Oncol. 2017;116:416–26.
11. Nejati R, Goldstein JB, Halperin DM, Wang H, Hejazi N, Rashid A, et al. Prognostic significance of tumor-infiltrating lymphocytes in patients with pancreatic ductal adenocarcinoma treated with neoadjuvant chemotherapy. Pancreas. 2017;46:1180–7.
12. Takeuchi S, Baghdadi M, Tsuchikawa T, Wada H, Nakamura T, Abe H, et al. Chemotherapy-derived inflammatory responses accelerate the formation of immunosuppressive myeloid cells in the tissue microenvironment of human pancreatic cancer. Cancer Res. 2015;75:2629–40.
13. Tsuchikawa T, Hirano S, Tanaka E, Matsumoto J, Kato K, Nakamura T, et al. Novel aspects of preoperative chemoradiation therapy improving anti-tumor immunity in pancreatic cancer. Cancer Sci. 2013;104:531–5.
14. Miyashita T, Tajima H, Makino I, Okazaki M, Yamaguchi T, Ohbatake Y, et al. Neoadjuvant chemotherapy with gemcitabine plus nab-paclitaxel reduces the number of cancer-associated fibroblasts through depletion of pancreatic stroma. Anticancer Res. 2018;38:337–43.
15. Kalluri R. The biology and function of fibroblasts in cancer. Nat Rev Cancer. 2016;16:582–98.
16. Ino Y, Yamazaki-Itoh R, Oguro S, Shimada K, Kosuge T, Zavada J, et al. Arginase II expressed in cancer-associated fibroblasts indicates tissue hypoxia and predicts poor outcome in patients with pancreatic cancer. PLoS ONE. 2013;8:e55146.
17. Armstrong T, Packham G, Murphy LB, Bateman AC, Conti JA, Fine DR, et al. Type I collagen promotes the malignant phenotype of pancreatic ductal adenocarcinoma. Clin Cancer Res. 2004;10:7427–37.
18. Berchtold S, Grunwald B, Kruger A, Reithmeier A, Hahl T, Cheng T, et al. Collagen type V promotes the malignant phenotype of pancreatic ductal adenocarcinoma. Cancer Lett. 2015;356:721–32.
19. Ohlund D, Franklin O, Lundberg E, Lundin C, Sund M. Type IV collagen stimulates pancreatic cancer cell proliferation, migration, and inhibits apoptosis through an autocrine loop. BMC Cancer. 2013;13:154.
20. Olivares O, Mayers JR, Gouirand V, Torrence ME, Gicquel T, Borge L, et al. Collagen-derived proline promotes pancreatic ductal adenocarcinoma cell survival under nutrient limited conditions. Nat Commun. 2017;8:16031.
21. Shields MA, Dangi-Garimella S, Krantz SB, Bentrem DJ, Munshi HG. Pancreatic cancer cells respond to type I collagen by inducing snail expression to promote membrane type 1 matrix metalloproteinase-dependent collagen invasion. J Biol Chem. 2011;286:10495–504.
22. Campbell TN, Attwell S, Arcellana-Panlilio M, Robbins SM. Ephrin A5 expression promotes invasion and transformation of murine fibroblasts. Biochem Biophys Res Commun. 2006;350:623–8.

23. Eisenhauer EA, Therasse P, Bogaerts J, Schwartz LH, Sargent D, Ford R, et al. New response evaluation criteria in solid tumours: revised RECIST guideline (version 1.1). Eur J Cancer. 2009;45:228–47.
24. Brierley JD, Gospodarowicz MK, Wittekind C. *TNM classification of malignant tumours*, 8th ed. Wiley-Blackwell: Hoboken, NJ, 2017.
25. Japan-Pancreas-Society. *Classification of Pancreatic Cancer*, 3rd English ed. Kanehara: Tokyo, Japan, 2011.
26. Hiraoka N, Ino Y, Hori S, Yamazaki-Itoh R, Naito C, Shimasaki M, et al. Expression of classical human leukocyte antigen class I antigens, HLA-E and HLA-G, is adversely prognostic in pancreatic cancer patients. Cancer Sci. 2020;111:3057–70.
27. Oguro S, Ino Y, Shimada K, Hatanaka Y, Matsuno Y, Esaki M, et al. Clinical significance of tumor-infiltrating immune cells focusing on BTLA and Cbl-b in patients with gallbladder cancer. Cancer Sci. 2015;106:1750–60.
28. Ramilowski JA, Goldberg T, Harshbarger J, Kloppmann E, Lizio M, Satagopam VP, et al. A draft network of ligand-receptor-mediated multicellular signaling in human. Nat Commun. 2015;6:7866.
29. Ino Y, Oguro S, Yamazaki-Itoh R, Hori S, Shimada K, Hiraoka N. Reliable evaluation of tumor-infiltrating lymphocytes in pancreatic cancer tissue biopsies. Oncotarget. 2019;10:1149–59.
30. Doi N, Ino Y, Angata K, Shimada K, Narimatsu H, Hiraoka N. Clinicopathological significance of core 3 O-glycan synthetic enzyme, beta1,3-N-acetylglucosaminyltransferase 6 in pancreatic ductal adenocarcinoma. PLoS ONE. 2020;15:e0242851.
31. Imamura T, Iguchi H, Manabe T, Ohshio G, Yoshimura T, Wang ZH, et al. Quantitative analysis of collagen and collagen subtypes I, III, and V in human pancreatic cancer, tumor-associated chronic pancreatitis, and alcoholic chronic pancreatitis. Pancreas. 1995;11:357–64.
32. Julich D, Mould AP, Koper E, Holley SA. Control of extracellular matrix assembly along tissue boundaries via Integrin and Eph/Ephrin signaling. Development. 2009;136:2913–21.
33. Lagares D, Ghassemi-Kakroodi P, Tremblay C, Santos A, Probst CK, Franklin A, et al. ADAM10-mediated ephrin-B2 shedding promotes myofibroblast activation and organ fibrosis. Nat Med. 2017;23:1405–15.
34. Walsh R, Blumenberg M. Specific and shared targets of ephrin A signaling in epidermal keratinocytes. J Biol Chem. 2011;286:9419–28.
35. Chang Q, Jorgensen C, Pawson T, Hedley DW. Effects of dasatinib on EphA2 receptor tyrosine kinase activity and downstream signalling in pancreatic cancer. Br J Cancer. 2008;99:1074–82.
36. Duxbury MS, Ito H, Zinner MJ, Ashley SW, Whang EE. EphA2: a determinant of malignant cellular behavior and a potential therapeutic target in pancreatic adenocarcinoma. Oncogene. 2004;23:1448–56.
37. Pasquale EB. Eph receptors and ephrins in cancer: bidirectional signalling and beyond. Nat Rev Cancer. 2010;10:165–80.
38. Himanen JP, Chumley MJ, Lackmann M, Li C, Barton WA, Jeffrey PD, et al. Repelling class discrimination: ephrin-A5 binds to and activates EphB2 receptor signaling. Nat Neurosci. 2004;7:501–9.
39. Pasquale EB. The Eph family of receptors. Curr Opin Cell Biol. 1997;9:608–15.
40. Giaginis C, Tsourouflis G, Zizi-Serbetzoglou A, Kouraklis G, Chatzopoulou E, Dimakopoulou K, et al. Clinical significance of ephrin (eph)-A1, -A2, -a4, -a5 and -a7 receptors in pancreatic ductal adenocarcinoma. Pathol Oncol Res. 2010;16:267–76.
41. Mudali SV, Fu B, Lakkur SS, Luo M, Embuscado EE, Iacobuzio-Donahue CA. Patterns of EphA2 protein expression in primary and metastatic pancreatic carcinoma and correlation with genetic status. Clin Exp Metastasis. 2006;23:357–65.
42. Markosyan N, Li J, Sun YH, Richman LP, Lin JH, Yan F, et al. Tumor cell-intrinsic EPHA2 suppresses anti-tumor immunity by regulating PTGS2 (COX-2). J Clin Invest. 2019;129:3594–609.
43. Lee CS, Montebello J, Georgiou T, Rode J. Distribution of type IV collagen in pancreatic adenocarcinoma and chronic pancreatitis. Int J Exp Pathol. 1994;75:79–83.
44. Desgrosellier JS, Cheresh DA. Integrins in cancer: biological implications and therapeutic opportunities. Nat Rev Cancer. 2010;10:9–22.
45. Grzesiak JJ, Bouvet M. The alpha2beta1 integrin mediates the malignant phenotype on type I collagen in pancreatic cancer cell lines. Br J Cancer. 2006;94:1311–9.
46. Dauer P, Zhao X, Gupta VK, Sharma N, Kesh K, Gnamlin P, et al. Inactivation of cancer-associated-fibroblasts disrupts oncogenic signaling in pancreatic cancer cells and promotes its regression. Cancer Res. 2018;78:1321–33.

ACKNOWLEDGEMENTS

We thank Ms. Sachiko Miura and Toshiko Sakaguchi for excellent techniques. We also thank Fumiyo Saito (Chemical Evaluation Research Institute, Tokyo, Japan) for bioinformatic analysis. The authors are grateful to the Mr. Naoki Kimoto, Mr. Koichiro Horiguchi, and Ms. Miyuki Kubokawa (Amelieff, Tokyo, Japan) to modify the software program, and Naoko Tominaga (Dnaform, Kanagawa, Japan) to extract CAGE data in this study. We are grateful to the National Cancer Center Biobank for the tissue samples used in this study.

AUTHOR CONTRIBUTIONS

Study concept and design; KN and NK, acquisition of data, analysis and interpretation of data; KN, YI, CN, SN, MS, UI, TI, ND and NH, drafting of the manuscript; KN, critical revision of the manuscript for important intellectual content; NH, obtained funding; KN and NH, technical or material support; ME, YK, KS and NH, study supervision; NH.

FUNDING

This work was supported by JSPS KAKENHI [21K07139(NH), 18K16377(KN)], and AMED [21ck0106540(NH)].

COMPETING INTERESTS

The authors declare no competing interests.

ETHICS APPROVAL AND CONSENT TO PARTICIPATE

This study was approved by the Institutional Review Board of the National Cancer Center, Japan (#2005-077 and #2016-006). Informed consent was obtained from all participants involved in the study, and all clinical investigations were conducted in line with the principles of the Declaration of Helsinki.

CONSENT TO PUBLISH

There are no individual person's data from all participants involved in the study.

ADDITIONAL INFORMATION

Supplementary information The online version contains supplementary material available at https://doi.org/10.1038/s41416-021-01639-9.

Correspondence and requests for materials should be addressed to Nobuyoshi Hiraoka.

Reprints and permission information is available at http://www.nature.com/reprints

Publisher's note Springer Nature remains neutral with regard to jurisdictional claims in published maps and institutional affiliations.